11 NMR/NQR Spectroscopy

D. Brinkmann, S. Berger, M. Mali, R. Pozzi, F. Raffa, J. Roos, A. Suter, and A. Zavidonov .
Diploma students: M. Foglia, U. Lehmann, J. Plaz.
Guests: Dr. M. Igarashi, Gunma College of Technology, Gunma (Japan), till September 1998; Prof. M. Itoh, Chiba University (Japan), April - August 1998; Dr. I.A. Larionov, Kazan State University (Russia), since October 1998; I. Eremin, Kazan State University (Russia), December 1998; Prof. K.N. Shrivastava, University of Hyderabad (India), February 1999.

This is the last Annual Report of the Physics Institute's NMR/NQR group in its present constitution. The 1998/1999 period has been dominated by all Ph.D. students finishing their theses and writing their final research papers, and the diploma students taking their final examinations. As in previous years, we have employed NMR/NQR techniques to probe, at a *microscopic* level, advanced materials like high–temperature superconductors, their antiferromagnetic parent compounds, and superionic conductors. One of the special techniques has been high-pressure NMR/NQR. Our major recent results will be summarized below.

11.1 Colloquium on *MAGNETIC RESONANCE IN HIGH-T_c SUPERCONDUCTORS*

After 12 years of ever increasing magnetic resonance activity in the field of high-T_c superconductors, we thought that a gathering of people involved in this research is appropriate and useful. We organized a small, well-focused meeting (in the spirit of our 1991 Colloque AMPERE with a similar title) which provided a general overview of the present state of the art of NMR, NQR, and EPR studies in high-temperature superconductors. Or in simple words: "What have we learnt so far about high-T_c superconductors from magnetic resonance studies?" The meeting also marked the end of our superconductor research of more than one decade.

The Colloquium took place in Engelberg from 17 through 22 January 1999 and it consisted of oral presentations (both invited and contributed) and private discussion. The meeting had been attended by about 35 scientists, many of them from abroad. We were pleased to see that the participants regarded the Colloquium as highly successful and very stimulating.

11.2 High-temperature superconductors

The topics of this project are central issues in this field of research and are all dealing with Y–Ba–Cu–O superconductors: the isotope effect of the spin gap, the inter–plane electronic spin polarization transfer in the superconducting state, the spin and charge dynamics in Cu–O chains combined with a theoretical study of the magnetic properties of these chains, and the cluster formation of chain oxygen vacancies and its relation to vortices.

11.2.1 Isotope effect of the spin gap

The work on the isotope effect of the spin gap has now been published [1]. We have shown by high-precision ^{63}Cu NQR spin-lattice relaxation experiments that the spin gap as characterized by the temperature $T^\star$ [where the relaxation rate per Kelvin reaches its maximum], is isotope dependent with an isotope exponent $\alpha_{T^\star} = 0.061(8)$ which agrees quite well with the corresponding exponent $\alpha_{T_c} = 0.056(12)$ for T_c as determined by SQUID magnetization measurements. This fact seems to confirm the growing evidence for a common origin of the superconductivity and the pseudo gaps. Finally, a possible relation between the opening of the spin gap and a CDW transition has been discussed.

On the other side, a quantitative prediction of an isotope dependence of the pseudo gap had been made within the charge-density wave (CDW) scenario; an isotope exponent $\alpha_{T_{\rm CDW}} = 0.028$ has been calculated which is roughly a factor of 2 smaller than the experimental value. It is important to stress that according to this model, $\alpha_{T_{\rm CDW}}$ and α_{T^*} do not need to be identical. However, the result that both parameters are of the same order, is consistent with a possible relation between a CDW transition and the opening of the spin gap.

The group of Williams *et al.* [2] had claimed the absence of an isotope effect on the spin gap. After our paper has appeared, Williams *et al.* now report that their data also favor the isotope effect.

11.2.2 Spin and charge dynamics in the Cu–O chains of $YBa_2Cu_4O_8$

There is an increasing interest in the physics of hole-doped Cu–O chains, as they may play an essential role in the normal and superconducting states of the superconductors $YBa_2Cu_3O_7$ and $YBa_2Cu_4O_8$. We therefore have continued our study of $YBa_2Cu_4O_8$ by performing NQR-NMR experiments with its chain copper and apex oxygen [3].

Above T_c, the temperature dependences of the Cu spin-lattice relaxation rate and the Knight shift are quantitatively described within the framework of the one-dimensional electron gas model [4, 5], where the anisotropy and the correlation of the chain electron system are taken into account. Electric field gradient fluctuations due to charge carriers in the chains contribute partly to the chain Cu relaxation and dominate the apex oxygen relaxation. The different temperature dependences of the magnetic and quadrupolar relaxation rates of the chain Cu (see Figure 11.1) seem to confirm the separation of low energy spin and charge excitations (spin-charge separation), expected in the framework of the one-dimensional electronic gas model.

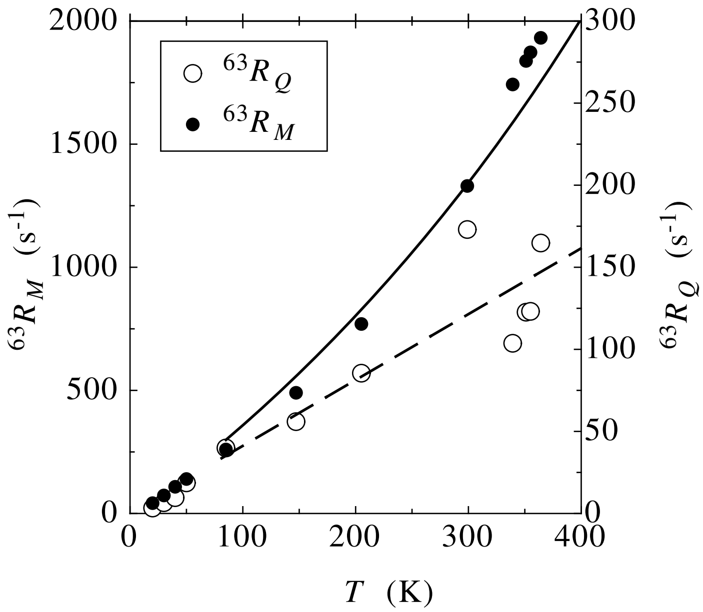

Figure 11.1: *Temperature dependence of the magnetic (R_M) and quadrupolar (R_Q) spin-lattice relaxation rate. The solid line is the result of the analysis based on the electron gas model. The dashed line is a guide to the eye.*

Finally, we showed that the drop in the chain's magnetic shift at T_c seems to be related to the occurrence of superconductivity in the chains through the proximity effect. Our experimental findings are not compatible with a charge density wave transition in the chains. Such a transition has been discovered in the chains of $PrBa_2Cu_3O_7$ and has been suggested for the chains of $YBa_2Cu_3O_7$.

11.2.3 Magnetic properties of Cu–O chains in $YBa_2Cu_3O_7$ and $YBa_2Cu_4O_8$

A different and more sophisticated approach to understand hole–doped chains in Y–Ba–Cu–O superconductors is the following. It is known that, in one-dimension, the Fermi-liquid paradigm, based on the quasi-particle picture, breaks down and leads to anomalies of the magnetic properties. It is believed that the Luttinger-liquid approach is most appropriate for the description of the properties of 1D quantum systems [6]. This approach implies that the low-energy spectrum of the real 1D quantum system can be reproduced by the effective Luttinger-Tomonaga model which can be solved exactly [7].

Mapping the one-dimensional Hubbard model into the Luttinger–Tomonaga model, we have calculated the temperature dependencies of the chain copper nuclear magnetic spin–lattice relaxation rate and Knight shift for the normal state of the superconducting materials $YBa_2Cu_3O_7$ and $YBa_2Cu_4O_8$ [8]. The dynamic spin susceptibility has been calculated by using a bosonization technique and results of the renormalization group analysis for the one-dimensional quantum systems. A comparison of our results with NMR data shows that the model is able to reproduce the main features of the spin dynamics in both materials. The set of fit parameters have reasonable values for both compounds and are naturally connected with each other.

11.2.4 Interplane electronic spin polarization transfer in the superconducting state of $Y_2Ba_4Cu_7O_{15}$

Superconductivity in Y–Ba–Cu–O compounds takes place in the CuO_2 planes which form double planes or bilayers. The coupling between individual planes of a bilayer and its influence on the spin dynamics are one of the most important topics in present research. In the past, we have performed extensive NQR/NMR studies of $Y_2Ba_4Cu_7O_{15}$ (2–4–7) by measuring various planar Cu NQR/NMR parameters such as different relaxation times and the Knight shift. We also have used NQR spin–echo double resonance (SEDOR) to confirm independently and directly the existence of the inter–plane coupling in 2–4–7 and have determined the temperature dependence of the inter–plane component of the static electron spin susceptibility in the normal state.

We have then extended those studies into the superconducting phase by again performing SEDOR NQR with the planar Cu sites in 2–4–7 [9]. The detailed analysis of the temperature dependence of the indirect in–plane relaxation rate, R_2, and the inter–plane spin-spin relaxation rate, R_S^{inter}, reveals two results (see Figure 11.2): (i) In the normal conducting state, strong antiferromagnetic correlations exist between adjacent CuO_2 layers. (ii) In the superconducting state, the electronic spin polarization transfer between these layers is drastically reduced for decreasing temperature. Both results together strongly favor the interlayer tunneling model of P.W. Anderson and his colleagues.

11.2.5 Cluster formation of chain oxygen vacancies in $YBa_2Cu_3O_{7-\delta}$ as the origin of the fishtail anomaly

There is an anomaly in the irreversible magnetization hysteresis curve in single crystals of $YBa_2Cu_3O_7$, often referred to as “fishtail effect”: the magnetization increases anomalously on increasing the magnetic field. This feature is still of particular interest since the high

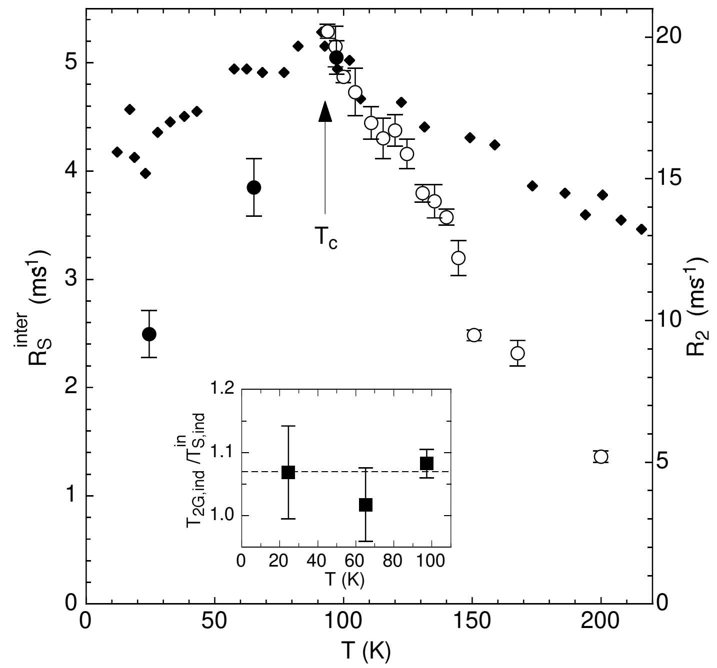

Figure 11.2: *Temperature dependence of the relaxation rates in $Y_2Ba_4Cu_7O_{15}$. Left scale: $R_S^{\rm inter}$ for the experiment $I = {}^{63}{\rm C}u(2), S = {}^{63}{\rm C}u(3)$ (open circles, our previous work) and for $I = {}^{63}{\rm C}u(3), S = {}^{63}{\rm C}u(2)$ (bullets). Right scale: R_2 of ^{63}Cu(3) (black diamonds, previous work). The vertical arrow denotes T_c. The inset shows $T_{2G,{\rm ind}}/T_{S,{\rm ind}}^{\rm in}$ vs. temperature for the 1-2-4 block, where $T_{2G,{\rm ind}}$ refers to ^{63}Cu(3) and $T_{S,{\rm ind}}^{\rm in}$ to the I-spin ^{65}Cu(3). The dashed line is a theoretical prediction.*

critical currents calculated from the maximum of the magnetization curve suggests that even at high fields large critical currents can be passed through this material.

It is a striking feature of *highly pure single crystals* of $YBa_2Cu_3O_{6.9}$ (1–2–3–6.9) that the fishtail effect can be switched off and on in a reversible manner by changing the annealing temperature. Erb *et al.* [10] have proposed the following model. Annealing the crystal at 510 K (and 1 bar oxygen pressure) causes clustering of the oxygen vacancies and the clusters form pinning centers which then lead to the fishtail effect. However, annealing the same sample at 650 K (and 100 bar), produces a random distribution of the vacancies which are now too small to act as pinning centers. In $YBa_2Cu_3O_7$, no fishtail effect could be observed due to the absence of vacancies.

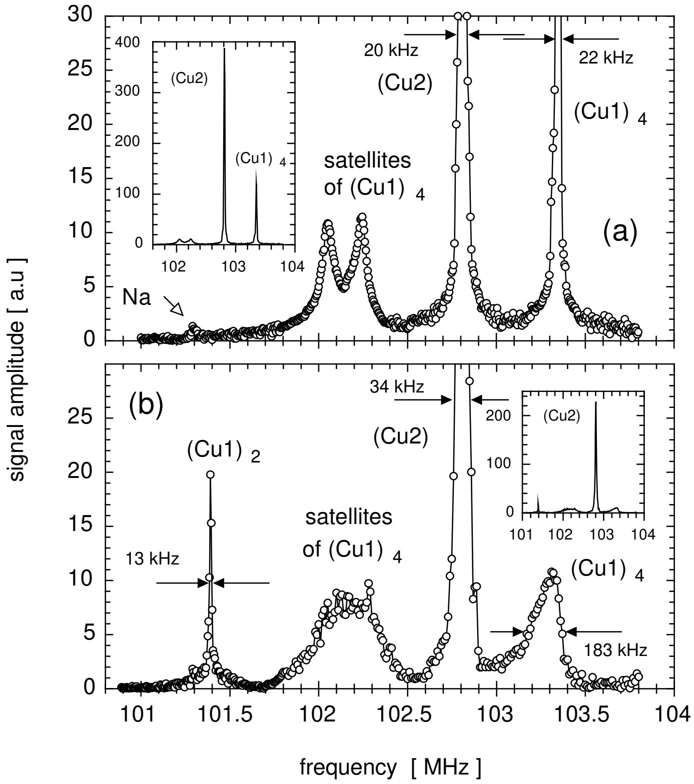

Figure 11.3: ^{63}Cu *central (and satellite) lines of different sites are shown (a) for* $YBa_2Cu_3O_7$ *and (b) for* $YBa_2Cu_3O_{6.9}$ *at room temperature. The index denotes the oxygen coordination of the respective Cu site. The external magnetic field (8.995 Tesla) was oriented along the c-axis of the single crystal. The insets show the full size of the lines.*

We have completed an extended series of Cu NMR and NQR (see *e.g.* Figure 11.3) to check the vacancy cluster hypothesis [11]. Together with magnetization measurements and positron annihilation spectroscopy, we found evidence that the formation of oxygen vacancy clusters is the origin of the fishtail anomaly in $YBa_2Cu_3O_{7-\delta}$. Note that single vacancies or point defects cannot be responsible for the anomaly, since the anomaly can also be suppressed in the optimally doped state where vacancies are present. Thus, a formation mechanism that leads to larger nevertheless still microstructural inhomogeneities must be responsible for this effect. In the case of $YBa_2Cu_3O_{7.0}$, the anomaly is intrinsically absent unless the crystals contain metallic impurities. In such $YBa_2Cu_3O_{7.0}$ samples, melting of the vortex lattice has been observed by calorimetric measurements as a first order transition between 4 and 26.5 T, which was the highest available field, giving further support for our interpretation and yields new insight into the nature of the vortex matter.

What is still missing is the NMR/NQR evidence for the "inverse effect": if the fishtail effect is absent, the NMR/NQR spectra should display the corresponding signals. However, it is difficult to suppress the fishtail effect completely in the large samples needed for the NMR/NQR experiments.

11.3 Antiferromagnetic parent compounds

There is a twofold interest in the electronic and magnetic structure of antiferromagnetic (AF) parent compounds from which many high–temperature superconductors are derived. First, there is the question about a possible interplay between magnetism and superconductivity. Even if there is no direct relation between magnetism and the mechanism of superconductivity, magnetism in these compounds certainly reflects the strong electronic correlation that exists and that must be taken into account in any attempt to explain electron pairing in cuprates. Second, the crossover between two–dimensional (2D) and three–dimensional (3D) magnetic systems offers insight into the spin dynamics of a so–called spin-1/2 2D quantum Heisenberg AF. We have continued these investigations by some general considerations of all these AF compounds and by a very detailed study of the bilayered $YBa_2Cu_3O_6$.

11.3.1 Sublattice magnetization in the antiferromagnetic parent compounds

The 3D ordered state of the AF parent compounds is a peculiar state with extreme anisotropic exchange couplings. One of the most important features of this AF state are the magnon excitations which can be studied via the temperature dependence of the sublattice magnetization, $M(T)$. Especially suited for these investigations is NMR in zero external magnetic field, a technique we have employed for several years, since the NMR Larmor frequency is a measure of $M(T)$.

The three antiferromagnets La_2CuO_4, $YBa_2Cu_3O_6$, and $Ca(Sr)CuO_2$ exhibit a common feature: the temperature dependence of the relative decrease of $M(T)$ follows a power law, that is $[M(0) - M(T)]/M(0) = AT^n$, up to one-half of the Néel temperature (T_{N}) with the same power, $n \sim 2$; only the prefactor A differs from compound to compound. This behavior of $M(T)$ suggests a common mechanism responsible for the decrease.

We have now performed the missing *numerical* calculation of $M(T)$ for $Ca(Sr)CuO_2$ [12] using the spin-wave model applied to a quasi-2D Heisenberg antiferromagnet (see Figure 11.4). We confirmed the experimental result that the power law is obeyed at temperatures below about $T_{\mathrm{N}}/2$. Thus, all three antiferromagnets are well described, in the respective temperature range, as quasi 2D S=1/2 Heisenberg systems with the inter–layer coupling constant, $J^{'}$, dominating the value of the prefactor A.

11.3.2 The paramagnetic phase of $YBa_2Cu_3O_6$

Although $YBa_2Cu_3O_6$ is the AF parent compound of the whole Y–Ba–Cu–O superconductor family, an adequate NMR study of the planar Cu(2) site in the *paramagnetic* phase has still been missing. This is due to severe experimental difficulties like the extremely short spin–spin and spin–lattice relaxation of the planar Cu(2) nuclei as well as its disadvantageous quadrupole coupling. Because now sufficiently large *single* crystals are available (synthesized by A. Erb, University of Geneva), we have extended our studies to a large temperature range, extending from slightly below $T_N \cong 410$ K up to nearly 1000 K [13]. Our major results are as follows.

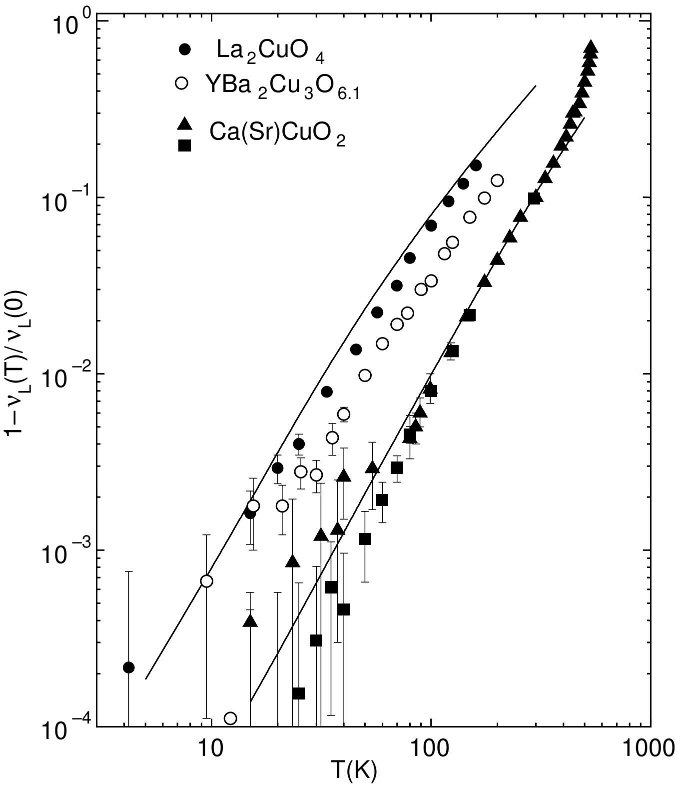

Figure 11.4: *The temperature dependence of the decrease of the Larmor frequency, $\nu_L(T)$, in La_2CuO_4, $YBa_2Cu_3O_{6.1}$, and $Ca(Sr)CuO_2$. The remeasured data for $Ca(Sr)CuO_2$ are shown by full squares. The solid lines for La_2CuO_4 and $Ca(Sr)CuO_2$ represent theoretical values calculated by means of the linear spin-wave model.*

Above 500 K, the Cu(2) relaxation data reveal that $YBa_2Cu_3O_{6.12}$ is in the renormalized classical (RC) regime of a 2D quantum Heisenberg AF with spin S=1/2, what means that electron spins of neighboring planes fluctuate independently. From the data, we calculated the temperature dependence of the AF correlation length (see Figure 11.5) and determined a value for the hyperfine coupling constant at the Cu(2) site and the effective magnetic moment. We concluded that, among the antiferromagnets La_2CuO_4, $YBa_2Cu_3O_6$, and $Ca_{0.85}Sr_{0.15}CuO_2$, the value of the effective magnetic moment is larger the stronger the magnetic inter–plane coupling. Above 600 K, the Cu(2) hyperfine coupling constant exhibits an unusual change which is not yet explained. We inferred, from the Cu(1) relaxation above 500 K, that diffusion of remnant oxygen in the chains is present.

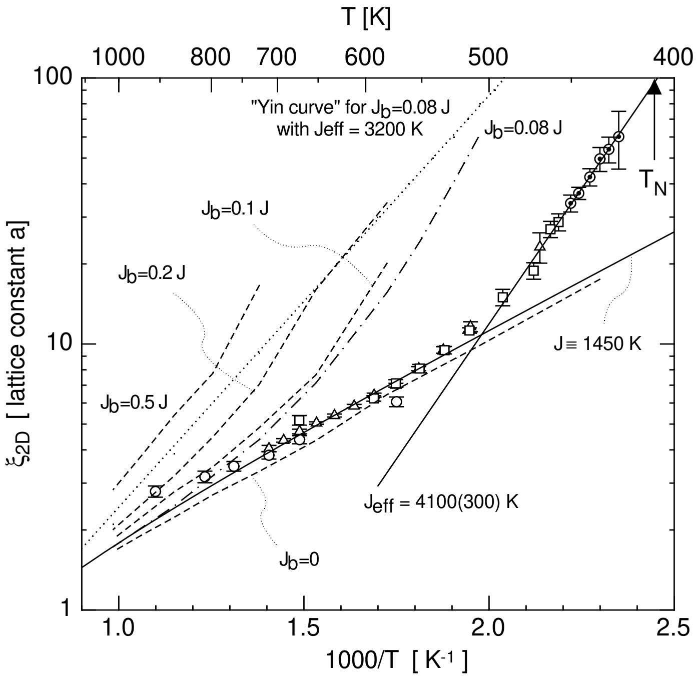

Figure 11.5: *The planar antiferromagnetic correlation length, ξ_{2D}, as a function of inverse temperature. The solid lines are fits to the experimental data at high temperature and above T_N, respectively. The dotted line represents the prediction for a S=1/2 bilayer quantum Heisenberg antiferromagnet in the renormalized classical regime with intra–bilayer coupling constant $J_b = 0.08J$. The dashed and dashed–dotted curves are the results of Quantum Monte Carlo calculations for bilayers with J_b ranging from 0.08J to 0.5J.*

Below 500 K, the individual layers in $YBa_2Cu_3O_{6.12}$ start to couple into pairs and the temperature dependence of the AF correlation length abruptly crosses over to a faster increase when T_N is approached. The corresponding effective AF in–plane coupling constant becomes J_{eff}=4100 K, a value nearly three times larger than J=1450 K known for the isolated layer. A comparison with Quantum Monte Carlo calculations allows one to estimate an intra–bilayer coupling constant, $J_b/J \lesssim 0.01$, which is significantly smaller than $J_b/J = 0.08$ as obtained by neutron scattering experiments. The origin of this disagreement is not yet known. Only $\approx$ 5 K above T_N, also the bilayers begin to couple as indicated by a suppression of the Cu(1) relaxation rate.

The decoupling of the planes adds, at least partially, to the unusual increase of the ^{89}Y relaxation rate above 425 K. This rate enhancement with rising temperature was measured previously and was not fully understood.

Measuring the susceptibility anisotropy, we detected a crossover in the Cu(2) spin fluctuations. In the range $T_N \pm$ 5 K, these fluctuations are XY–like and become, with rising temperature, increasingly isotropic; the crossover is already complete around 500 K. This behavior is similar to the crossover we observed recently in $Ca_{0.85}Sr_{0.15}CuO_2$.

The Néel temperature of $YBa_2Cu_3O_{6.12}$ does not depend on the orientation of the applied magnetic field of 5.16 Tesla. This behavior contrasts with that of $Sr_2CuO_2Cl_2$ where the orientational dependence of T_N is a consequence of its low value, namely 257 K.

11.4 Superionic glasses

11.4.1 Relaxation of the stationary phosphorus nucleus

Our investigation of lithium conducting phosphate glasses of composition xLiF$\cdot(1-x)$LiPO$_3$ has been motivated by the fact that addition of the dopant salt, LiF, enhances the conductivity; hence, we became interested in the microscopic counterpart of this effect. While previously dealing with ^{7}Li, ^{6}Li, and ^{19}F nuclei, we then turned to the nucleus, ^{31}P, of the stationary phosphorus ion. After studying the undoped sample, we now completed the investigations of doped samples [14].

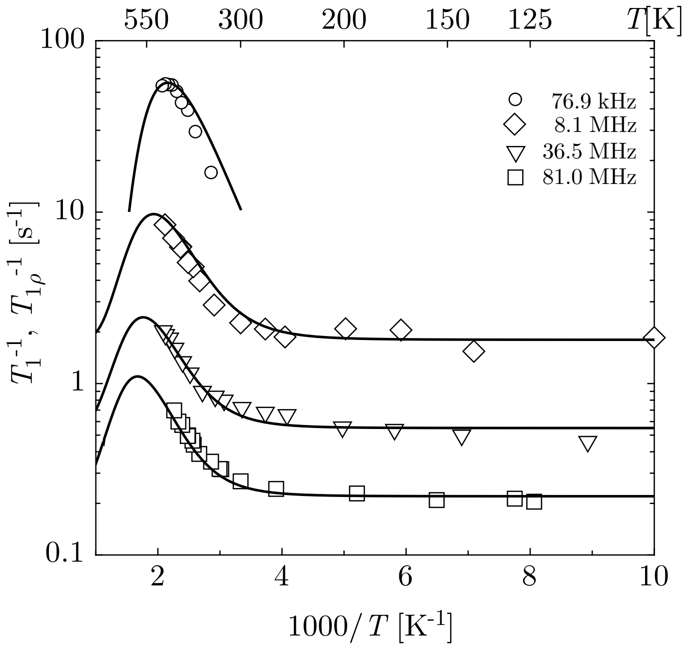

Figure 11.6: *Temperature dependent* ^{31}P *spin–lattice relaxation rates in* 0.35LiF$\cdot$0.65LiPO$_3$ *at various frequencies. Rates at 76.9 kHz have been measured in the rotating frame, the others in the laboratory frame.*

Parameters of the lithium motion could be extracted from the ^{31}P NMR since the ^{31}P spin–lattice relaxation is driven by magnetic fluctuations due to lithium ion motion. For modelling the temperature and frequency dependence of the spin–lattice relaxation rates, we employed the Bloembergen–Purcell–Pound theory modified with a Gaussian distribution of activation energies for the lithium motion. This distribution function takes care of the intrinsic disorder of the glass. We achieved to describe the relaxation data in the rotating frame as well as in the laboratory frame of reference with the *same* parameter set, thereby covering a wide frequency range from about 30 kHz to 80 MHz (see Figure 11.6). For both samples, the values for the center of the activation energy distribution agree very well with results obtained by DC conductivity measurements. The increase of the distribution width with increasing LiF content is attributed to a larger variety of lithium sites in the doped sample. These results demonstrate that even a "simple" relaxation model allows considerable insight into the ion dynamics. At low temperature, the relaxation rates evidence augmented network dynamics in the doped sample which is in accordance with the lower value of the glass transition temperature.

11.4.2 Magic angle spinning

Magic angle spinning (MAS) makes the time averaged dipolar coupling in a solid to vanish; it eliminates chemical shift anisotropies and first–order quadrupole couplings. In order to investigate the influence of doping on the structural change of the glassy network in xLiF$\cdot(1-x)$LiPO$_3$, we have now employed ^{31}P MAS [15] to samples with x between 0 and 0.35 (see Figure 11.7).

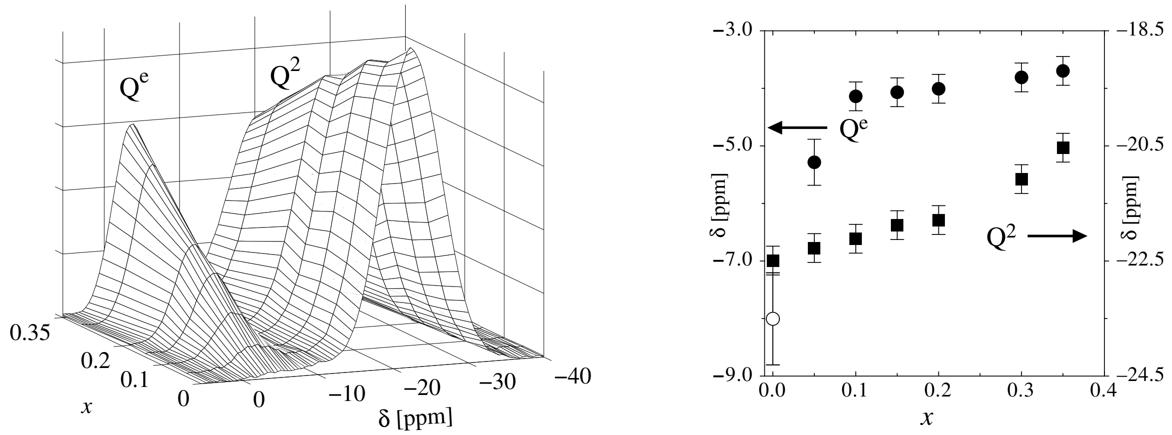

Figure 11.7: ^{31}P *MAS in* xLiF$\cdot(1-x)$LiPO$_3$. *Left: Spectra. Right: Isotropic chemical shift, δ, of phosphate end groups (Q^e, ●, left axis) and middle units (Q^2, ■, right axis) as a function of x. The open circle refers to Q^1 tetrahedra in undoped* LiPO$_3$.

Usually, the phosphate glass structure is described by Q^n groups which are basic structure units (PO$_4$ tetrahedra) where n is the number of bridging oxygens per PO$_4$ tetrahedron. The MAS spectra obtained at room temperature reveal two peaks. The former peak is attributed to Q^e tetrahedra (end groups) while the latter is a superposition of mid-chain and cyclic Q^2 phosphates. With increasing LiF content the number of end units increases whereas the number of cyclic/mid-chain phosphate groups is reduced.

11.4.3 ^{31}P–^{19}F spin–echo double resonance (SEDOR)

We have resumed our study of the stationary fluorine ions by performing new ^{19}F NMR experiments in 0.3LiF$\cdot$0.7LiPO$_3$. One part of the fluorine ions substitutes bridging oxygens in a PO$_4$ tetrahedron leading to structural depolymerization by creating PO$_3$F chain–end groups. The other part of the fluorine ions is embedded in the glassy structure as Li$^+$F$^-$ fragments. Both types of ions show up in the ^{19}F NMR spectrum as resonance lines with different chemical shifts (see "Left" of Figure 11.8). The spectrum has been fitted by three

Gaussian curves, A1, A2, and A3; the latter curve has been introduced because of the asymmetry of the spectrum at higher frequency. In the literature so far, the assignment of the two fluorine lines was simply based on the similarity of their shifts with ^{19}F shifts observed in other fluorinated phosphate compounds.

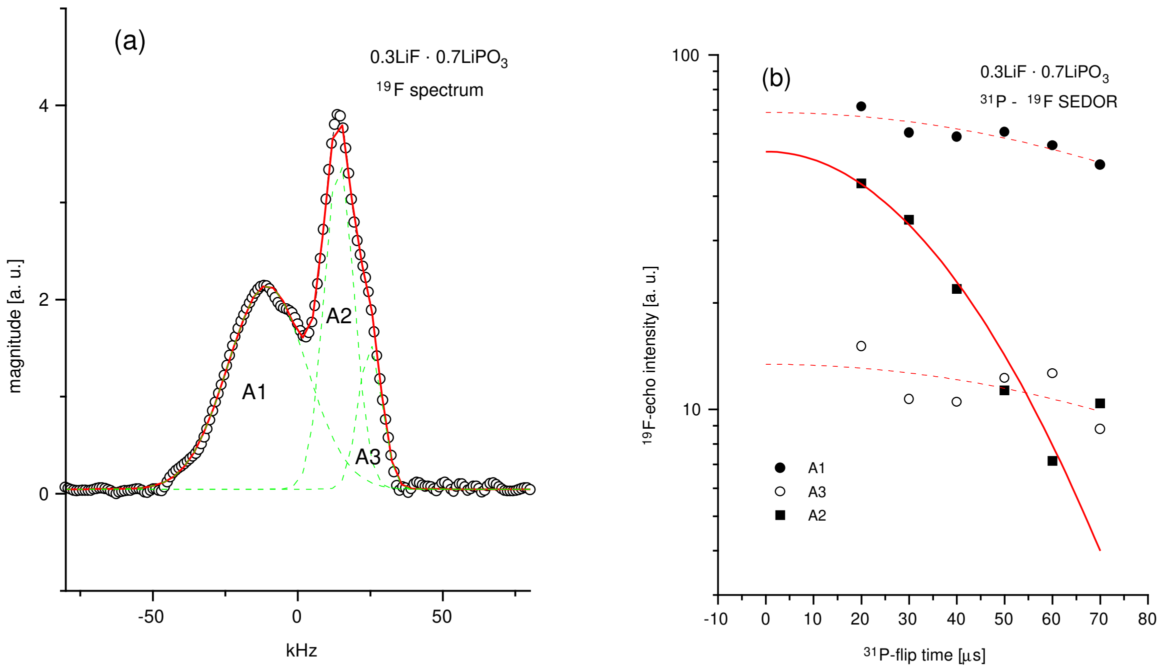

Figure 11.8: ^{31}P–^{19}F *spin–echo double resonance (SEDOR) experiment in* $0.3LiF{\cdot}0.7LiPO_3$. *Left:* ^{19}F *spectrum with three signals A1, A2, and A3. Right: Decay of the three* ^{19}F *echo signals if the* ^{31}P *spin is flipped.*

We obtained a more direct proof for the line assignment by performing a ^{31}P–^{19}F spin–echo double resonance (SEDOR) experiment which directly yields the second moment of the heteronuclear dipolar coupling between ^{31}P and ^{19}F nuclear spins; the moment is highly dependent on the distance between these nuclei, $r_{\mathrm{P\text{-}F}}$, via a term $(r_{\mathrm{P\text{-}F}})^{-6}$. The second moment leads to a decay of the echo intensity as observed in the measurement (see "Right" of Figure 11.8). The much stronger echo decay of line A2 compared to the two others immediately shows that the corresponding fluorine nuclei are closest to the phosphorus nuclei. Hence, fluorine nuclei yielding line A2 have to be assigned to PO_3F tetrahedra and lines A1 and A3 to the Li^+F^- fragments which are more distant to the central phosphorus atom of the PO_4 tetrahedra.

11.5 High–pressure NMR in $Ca_{0.85}Sr_{0.15}CuO_2$

Last year, we had reported on high–pressure studies of the antiferromagnet $Ca_{0.85}Sr_{0.15}CuO_2$ (CASCO) using our helium-pressure device. We have studied this compound very intensively before by other NMR/NQR techniques.

Having improved our diamond-anvil cell device, we now extended our CASCO studies to pressures beyond 0.7 GPa. Our objective is to determine the variation of the sublattice magnetization with pressure, that is in the antiferromagnetic phase. By employing the internal magnetic field, one performs ^{63}Cu NMR without an external magnetic field; the Larmor frequency is a measure for the sublattice magnetization. Between 1 and 2 GPa, we measured an increase of the magnetization with increasing pressure; this is in accord with our results from the helium-pressure experiments below 0.7 GPa. However, beyond 2 GPa we observed a decrease of the magnetization. This is very difficult to understand and it might be due to a technical defect. Thus, further experiments are needed in that pressure range before a final conclusion can be drawn.

References

[1] F. Raffa, T. Ohno, M. Mali, J. Roos, D. Brinkmann, K. Conder, and M. Eremin, Phys. Rev. Lett. 81 (1998) 5912

[2] G.V.M. Williams, J.L. Tallon, J.W. Quilty, H.J. Trodahl, and N.E. Flower, Phys. Rev. Lett. 80 (1998) 377

[3] F. Raffa, M. Mali, A. Suter, A. Yu. Zavidonov, J. Roos, D. Brinkmann, and K. Conder, submitted to Phys. Rev. B

[4] J. Solyom, Adv. Phys. 28 (1979) 201; V. J. Emery, in *Highly Conducting One-Dimensional Solids*, edited by J. T. Devreese, R. P. Evrard, and V. E. van Doren (Plenum, New York and London, 1979) Chap. 6

[5] C. Bourbonnais, P. Wzietek, F. Creuzet, D. Jérome, P. Batail, and K. Bechgaard, Phys. Rev. Lett. 62 (1989) 1532; C. Bourbonnais, J. Phys. I France 3 (1993) 143

[6] V. J. Emery, in *Highly Conducting One Dimensional Solids*, edited by J. T. Devreese *et al.* (Plenum Press, New York, 1978)

[7] D. C. Mattis and E. H. Lieb, J. Math. Phys. 6 (1965) 304

[8] A. Yu. Zavidonov and D. Brinkmann, to be submitted to Phys. Rev. B

[9] A. Suter, M. Mali, J. Roos, and D. Brinkmann, Phys. Rev. Lett. 82 (1999) 1309

[10] A. Erb, J.Y.Genoud, F. Marti, M. Däumling, E. Walker, and R. Flükiger, J. Low Temp. Phys. 105 (1996) 1033

[11] A. Erb, A. A. Manuel, M. Dhalle, F. Marti, J.-Y. Genoud B. Revaz, A.Junod, D.Vasumathi, S Ishibashi, A. Shukla, E Walker, Ø. Fischer, R.Flükiger, R. Pozzi, M. Mali, and D. Brinkmann, submitted to Phys. Rev. Lett.

[12] M.Matsumura, F.Raffa, and D. Brinkmann, submitted to Phys. Rev. B

[13] R. Pozzi, M. Mali, D. Brinkmann, A. Erb, and R. Flükiger, submitted to Phys. Rev. B

[14] S. Berger, J. Roos, A.Yu. Zavidonov,and D. Brinkmann, Solid State Ionics 112 (1998) 87

[15] S. Berger, M. Foglia, J. Roos, and D. Brinkmann, Joint 28th AMPERE - 13th ISMAR Conference, Berlin, August 2-7, 1998